



## Full Text View

[Volume 32, Issue 9 \(September 2002\)](#)

### Journal of Physical Oceanography

Article: pp. 2425–2440 | [Abstract](#) | [PDF \(1.65M\)](#)

# Lagrangian Eddy Scales in the Northern Atlantic Ocean

**Rick Lumpkin**

*Department of Oceanography, The Florida State University, Tallahassee, Florida, and Laboratoire de Physique des Océans, IFREMER, CNRS, Plouzane, France*

**Anne-Marie Treguier**

*Laboratoire de Physique des Océans, IFREMER, CNRS, Plouzane, France*

**Kevin Speer**

*Department of Oceanography, The Florida State University, Tallahassee, Florida*

(Manuscript received April 12, 2000, in final form December 3, 2001)

DOI: 10.1175/1520-0485(2002)032<2425:LESITN>2.0.CO;2

### ABSTRACT

Eddy time and length scales are calculated from surface drifter and subsurface float observations in the northern Atlantic Ocean. Outside the energetic Gulf Stream, subsurface timescales are relatively constant at depths from 700 m to 2000 m. Length scale and the characteristic eddy speed decrease with increasing depth below 700 m, but length scale stays relatively constant in the upper several hundred meters of the Gulf Stream. It is suggested that this behavior is due to the Lagrangian sampling of the mesoscale field, in limits set by the Eulerian eddy scales and the eddy kinetic energy. In high-energy regions of the surface and near-surface North Atlantic, the eddy field is in the “frozen field” Lagrangian sampling regime for which the Lagrangian and Eulerian *length* scales are proportional. However, throughout much of the deep ocean interior, the eddy field may be in the “fixed float” regime for which the Lagrangian and Eulerian *timescales* are nearly equal. This does not necessarily imply that the deep interior is nearly linear, as fixed-float sampling is possible in a flow field of  $O(1)$  nonlinearity.

### 1. Introduction

In this paper, we present and interpret the distribution of Lagrangian eddy scales measured by drifters and floats in the Northern Hemisphere of the Atlantic

#### Table of Contents:

- [Introduction](#)
- [Data](#)
- [Calculating eddy scales](#)
- [Observations](#)
- [Relating Lagrangian and Eulerian](#)
- [Discussion](#)
- [Concluding remarks](#)
- [REFERENCES](#)
- [APPENDIX](#)
- [FIGURES](#)

#### Options:

- [Create Reference](#)
- [Email this Article](#)
- [Add to MyArchive](#)
- [Search AMS Glossary](#)

#### Search CrossRef for:

- [Articles Citing This Article](#)

Search Google Scholar for:

Ocean. In recent years, the density of subsurface drifter observations has grown considerably, allowing far greater resolution of Lagrangian scale vertical distribution than previously published ([Böning 1988](#)). We also examine simulated drifters in a  $\frac{1}{3}^\circ$  eddy-permitting primitive equation model of the Atlantic, to help understand why the scales have their observed distribution.

- [Rick Lumpkin](#)
- [Anne-Marie Treguier](#)
- [Kevin Speer](#)

We must first define “Lagrangian eddy scales.” Consider a particle released into a fluid that subsequently moves at speed  $U(t)$ . This speed can be divided into a mean component  $U_o$ , which is the same for all particles passing through a fixed point (at any time), and a time-varying component  $u(t)$ , which varies from particle to particle. For a spatially homogeneous  $U_o$ , the position of the particle is  $X(t) = U_o t + x(t)$ , where

$$x(t) = \int_0^t d\tau u(\tau). \quad (1)$$

Assuming that  $u$  is ergodic, (1) can be used to derive Taylor's Theorem ([Taylor 1921](#)):

$$\langle x^2 \rangle = 2u'^2 \int_0^t d\tau (t - \tau) R(\tau), \quad (2)$$

where the dispersion  $\langle x^2 \rangle$  is an average over many particles of  $x^2$ ,  $u'$  is the characteristic eddy speed given by the standard deviation of  $u$ , and the velocity autocorrelation  $R$  is

$$R(\tau) = \lim_{T_m \rightarrow \infty} \frac{1}{u'^2 T_m} \int_0^{T_m} dt u(t) u(t + \tau). \quad (3)$$

The characteristic timescale of dispersion is the Lagrangian eddy timescale  $T_L$ ,

$$T_L = \int_0^\infty d\tau R. \quad (4)$$

This is the lag over which a particle's speed stays strongly correlated with itself. Because the particle moves at a characteristic speed  $u'$ , this timescale corresponds to a distance

$$L_L = u' T_L \quad (5)$$

called the Lagrangian eddy length scale. By analogy with Fickian diffusion,  $\langle x^2 \rangle$  can be related to an effective eddy diffusivity

$$\kappa_H = \frac{1}{2} \frac{d}{dt} \langle x^2 \rangle \quad (6)$$

([Taylor 1921](#); [Batchelor 1949](#)), which asymptotes to

$$\kappa_H = u' L_L \quad (7)$$

in the random-walk limit  $t \gg T_L$  (cf. [Davis 1982](#), [Garrett 1994](#)).

Early efforts to map  $\kappa_H$  from float observations in MODE (depth 1500 m) and LDE (700 m, 1400 m) found a diffusivity that varied with  $u'^2$ , consistent with an approximately constant timescale  $T_L \sim 7-9$  days (Price, in [Rossby et al. 1983](#) and [McWilliams et al. 1983](#)). [Poulain and Niiler \(1989\)](#) found a similar relationship for  $\kappa_H$  in the California Current System, but with a much shorter timescale (4.1–4.9 d). If a constant- $T_L$  rule (or, alternatively, a constant- $L_L$  rule) were universal, it would be of tremendous value: maps of  $\kappa_H$  could be estimated directly from the distribution of EKE ([Böning 1988](#)).

However, subsequent studies found that a constant- $T_L$  rule did not apply elsewhere. For near-surface drifters in the North Atlantic, diffusivity varied with  $u'$ , suggesting a constant length scale  $L_L \sim 31\text{--}39$  km (Krauss and Böning 1987). Brink et al. (1991) found a similar relationship (with  $L_L = 42$  km) for surface drifters in the California coastal transition zone, an energetic near-coast subset of the Poulain and Niiler (1989) study region. Böning (1988) used float observations at various depths to estimate the vertical distribution of  $T_L$  and  $L_L$  in the North Atlantic, and suggested that the floats encountered a depth-dependent, but  $u'$ -independent,  $L_L$  (i.e.,  $T_L \propto 1/u'$ ). Numerical simulations conducted by Hua et al. (1998) are also consistent with near-constant  $L_L$ . More recent drifter studies (Swenson and Niiler 1996; Lumpkin and Flament 2001) have found both  $L_L$  and  $T_L$  to vary with  $u'$  over large regions of the ocean surface. Clearly, neither a constant- $T_L$  nor a constant- $L_L$  rule is universal—but what are the dynamics that make them regionally applicable? Can we anticipate such rules in other regions of the ocean?

In the following sections, we present the observations used in this study (section 2), describe how eddy scales were calculated (section 3), and present the observed distribution of scales in the northern Atlantic (section 4). We then address why this distribution is observed by reviewing the relationship between Lagrangian and Eulerian scales (section 5) and examining the distribution of these scales in an eddy-permitting model (section 6). We speculate how these results may extend to the real ocean (section 7) and summarize our conclusions (section 8). In two appendices, we discuss alternative methods of calculating Lagrangian scales and discuss sources of scatter when comparing Lagrangian and Eulerian scales in the numerical model.

## 2. Data

Northern Atlantic surface drifter trajectories for 1989–97 were obtained from the Marine Environmental Data Service. The drifters were standard WOCE/SVP drifters (Niiler et al. 1987) with a holey-sock drogue centered at depth 15 m. A two-step quality evaluation algorithm was used to eliminate errors in the raw fixes, which were then interpolating to 1-day intervals via kriging (Hansen and Poulain 1996). The interpolated data spanned 738 drifter-years, with most observations concentrated between  $25^\circ$  and  $40^\circ\text{N}$  (Fig. 1). An important caveat of these drifters is that they follow the total (geostrophic and ageostrophic) near-surface flow, including Ekman drift. In regions where the wind-forced drift contributes significantly to eddy energy, Lagrangian scales derived from the total motion will be smaller than those derived from the geostrophic component alone. This effect should be least significant in currents such as the Gulf Stream and North Atlantic Current, where intense eddies and geostrophic mean flow dominate drifter motion. Farther north, where geostrophic eddy energy is weaker and winter storms can be intense, this effect may be pronounced.

Subsurface (SOFAR, RAFOS, and MARVOR) float trajectories were compiled from experiments in the tropical and northern Atlantic,<sup>1</sup> including two years of Eurofloats deployed in the deep northeastern Atlantic (Speer et al. 1999). A total of 588 float years were collected, spanning over 24 years from 1973 to 1998; 75% of observations deeper than 1000 m were made after 1985. The floats were at 90–4100 m, with half the observations concentrated in three narrow depth bins: 600–800 m (22% of data), 1000–1200 m (13%), and 1700–1900 m (15%).

## 3. Calculating eddy scales

Lagrangian scales were calculated from nonoverlapping 120-day segments of the float trajectories. Time series of zonal ( $u_1$ ) and meridional ( $u_2$ ) speeds were calculated for each trajectory segment via finite differencing. The mean and linear trend in the  $u_i$  were removed in order to minimize artificial magnification of the Lagrangian scales by shear in the pseudo-Eulerian mean flow field (cf. Krauss and Böning 1987). The autocorrelation functions  $R_{ii}$  were calculated using (3), with  $T_m = 120$  days. Because noise tends to dominate  $R$  for large lags, we followed the standard practice (cf. Freeland et al. 1975; Krauss and Böning 1987; Poulain and Niiler 1989) of integrating (4) to the first zero crossing.

These approximations to Eqs. (3) and (4) allow the maximum amount of data to be used in mapping the Lagrangian scales, but one should be aware of their effects. By removing the mean and linear trend of each 120-day segment, we discard low-frequency variability as well as the spatially varying mean field. With heavy sampling, such as in a regional deployment of a float cluster at one depth, one would prefer removing a time-mean flow, obtained by pseudo-Eulerian averaging of the floats and interpolated onto the individual trajectories. However, throughout much of the Atlantic, the full three-dimensional pseudo-Eulerian mean field is poorly resolved by the floats at scales finer than several degrees. By neglecting low-frequency variability, the scales  $T_L$  and  $L_L$  are artificially shortened. In contrast, truncating the integral in (4) at the first zero crossing of  $R$  tends to magnify  $T_L$  and  $L_L$  because  $R$  may have a prominent negative lobe beyond that crossing. In appendix A, we examine this second approximation by comparing alternative methods for approximating (4).

Horizontal averages (and their standard errors) of the eddy scales were calculated in  $10^\circ$  cells. Lagrangian scales from

each 120-day trajectory were treated as point measurements located at the trajectory's median longitude and latitude. Averages were not calculated where less than 10 estimates were obtained. Over 120 days, the average 1750-m-deep float traveled 150 km; 1.4% of the floats traveled over 1000 km in 120 days. The average surface drifter traveled 380 km in 120 days, and 14% traveled over 1000 km (2% experienced persistent mean currents greater than  $20 \text{ cm s}^{-1}$  over 120 days, thus traveling over 2000 km). We retained the trajectories spanning more than  $10^\circ$  in the averaging, although at least a small fraction of each consists of observations in neighboring cells; rejecting these trajectories would have biased the averages toward times of weak currents. As a consequence of retaining long trajectories, surface maps of the Lagrangian eddy scales may be “smoothed” along the direction of strong mean currents. In these maps, we shall present the average of the zonal and meridional components:  $u' = 0.5 \sum_i u'_{i,j}$ ,  $T_L = 0.5 \sum_i T_{L,i}$ ,  $L_L = 0.5 \sum_i L_{L,i}$ .

Maps of the scales' horizontal distribution shall be presented in two layers: surface (i.e., the near-surface WOCE drifters) and “deep,” the latter layer encompassing all floats between 1700 and 2000 m. We focus upon these two layers as they present well-sampled extremes in the oceanic EKE level. Observations at all depths were used to calculate the various scales' vertical distributions.

#### 4. Observations

[Figure 1](#) shows the apparent eddy diffusivity  $\kappa_H$  calculated via (7) for surface drifters and for floats deeper than 1500 m. Surface values of  $\kappa_H$  are nearly an order of magnitude larger than the deep values, reflecting the larger eddy energy and Lagrangian length scales at the surface. In both layers, the largest values are found in the western Atlantic. Surface values peak in the Gulf Stream extension, where the maximum value of  $22.8 \pm 1.8 \times 10^3 \text{ m}^2 \text{ s}^{-1}$  is found in the cell south of the Grand Banks. Regional surface maxima in  $\kappa_H$  extend along the path of the North Atlantic Current and the Azores Current (cf. [Fratantoni 2001](#)). Deep values are largest along the path of the deep western boundary current, and extremely small values of  $\kappa_H$ , averaging  $70 \pm 10 \text{ m}^2 \text{ s}^{-1}$ , are found in the deep eastern Atlantic south of  $50^\circ\text{N}$ .

[Figure 2](#) (top panels) shows  $T_L$  and  $L_L$  versus  $u'$  in the surface and deep layers of the northern Atlantic. The general tendency is for  $T_L$  to decrease, and  $L_L$  to increase, with increasing  $u'$ , as found in recent large-scale drifter studies ([Swenson and Niiler 1996](#); [Lumpkin and Flament 2001](#)). Unlike in the regional studies discussed earlier, neither a constant- $T_L$  or constant- $L_L$  “rule” characterizes the full set of observations.

Deep float observations are concentrated in three regions (see [Fig. 1](#)): the Gulf Stream extension region ([Owens 1991](#)), the MODE region ([Freeland et al. 1975](#); [Rossby et al. 1983](#)) (as defined here, a much broader region than that of MODE which encompasses the southwestern subtropics), and the eastern basin region of Eurofloat and ARCANE deployments ([Speer et al. 1999](#)). Vertical distributions of the Lagrangian scales in these regions are shown in [Fig. 3](#) (which may be compared with [Böning 1988](#), [Fig. 2](#)).

In all three regions,  $u'$  decreases by 2–2.5 times between the surface and 700–1000 m, and 1.5–2 times between 700 and 2000 m. In the “MODE” and “Eastern” basin regions,  $L_L$  has similar profiles. In the energetic Gulf Stream region,  $L_L$  decays by a barely significant 1.2 times (from 67 to 57 km) between the surface and 700 m. In all three regions, timescale  $T_L$  increases by 1.5–1.7 times between the surface and depth 700–1000 m; in the MODE and Eastern regions,  $T_L$  remains approximately constant (5.3–6.6 days) below 700 m, with the only significant change in subsurface  $T_L(z)$  between 1750 and 2150 m in the Eastern basin. In the Gulf Stream region,  $T_L$  is small (4.2 days) at 700 m, and increases a significant 1.3 times between 700 and 2150 m.

[Figure 4](#) shows the horizontal distribution of Lagrangian eddy scales. At the surface,  $T_L$  reaches its largest values ( $\sim 4$  days) in the center of the subtropical gyre and drops to smaller values in the far northern Atlantic. Surface  $L_L (=u' T_L)$  reaches maximum values of  $\sim 70$  km in the Gulf Stream. In the deep layer,  $T_L$  is smallest (4–6 days) in the eastern basin, and reaches maxima of  $\sim 9$  days in the Tropics. Deep  $L_L$  are 5–20 km, much smaller than at the surface.

At the surface, maxima in zonally averaged  $u'$  ([Fig. 5](#)) correspond to the locations of major currents (Gulf Stream, North Atlantic Current, and possibly the Azores Current), suggesting eddy generation by baroclinic instability ([Stammer 1997, 1998](#)). Peaks in zonally averaged  $L_L$  ([Fig. 6](#)) generally correspond to those in  $u'$  for both surface and deep observations. Variations in zonally averaged  $T_L$  ([Fig. 7](#)) show the surface maximum at  $30^\circ\text{N}$ .

#### 5. Relating Lagrangian and Eulerian scales

As a float passes through an eddy field, it mixes the field's spatial and temporal variability in its time series of displacement. The resulting relationship between  $T_L$  and  $T_E$  was quantified by [Middleton \(1985\)](#) for an idealized 2D, nondivergent, homogeneous, stationary eddy field. Middleton assumed Corrsin's (1950) conjecture and Gaussian mean-square Lagrangian displacements (the “parameterized Gaussian model” of [Davis 1982](#)). He found that the ratio  $T_L/T_E$  depends on the parameter  $u' / c_*$  (his  $\alpha$ , Davis'  $\tau_M/\tau_E$ ), where  $u'$  is the rms eddy speed and

$$c_* \equiv L_E/T_E \quad (8)$$

is the *evolution speed* of the eddy field, constructed from its Eulerian time and length scales. Middleton considered a wide range of possible statistics for the Eulerian field and showed that  $T_L/T_E$  could be predicted to within  $\sim 10\%$  by

$$T_L/T_E = q[q^2 + (u' / c_*)^2]^{-1/2}, \quad (9)$$

where  $q = (\pi/8)^{1/2}$ . Using the definition of  $L_L$ ,

$$L_L/L_E = (u' / c_*)[1 + (u' / c_*q)^2]^{-1/2}. \quad (10)$$

To visualize why the scales should be related according to (9) and (10), consider the two extremes of the Lagrangian sampling regime parameter  $u' / c_*$ . If  $u' / c_* < 1/2$ , a float travels a fraction of  $L_E$  before the current has changed substantially due to temporal fluctuations, so  $L_L < 0.4L_E$ . In this *fixed-float* regime, the float samples mesoscale fluctuations like a fixed current meter on a mooring:  $T_L \sim T_E$ . [Of course, because the float is not truly fixed, current meter and float time series of  $u(t)$  will diverge for  $t \gg T_L$ .] At the other extreme  $u' / c_* > 1$  [characterizing the [Davis \(1985\)](#) CODE observations], a float travels across many eddies before the field evolves significantly, so  $T_L < 0.5T_E$ . In this *frozen-field* regime,  $L_L \propto L_E$  because the eddy size determines the radii of curvature in the float trajectory's meanders. At intermediate values  $1/2 < u' / c_* < 1$ , both temporal and spatial variations of the Eulerian field play a lowest-order role in determining the Lagrangian scales.

## 6. Lagrangian and Eulerian scales in CLIPPER

In order to directly compare Eulerian and Lagrangian scales throughout the ocean, float observations were simulated in the CLIPPER North Atlantic primitive equation model ([Treguier et al. 1999, 2001](#)). The model uses an isotropic Mercator C-grid of  $1/3^\circ$  resolution at the equator with a corresponding grid size ranging from 37 km (equator) to 12.6 km ( $70^\circ\text{N}$ ). It has 42 vertical layers extending to a maximum depth of 5500 m with spacing increasing smoothly from 12 m (surface) to 200 m (below 1000 m). The model domain is  $75^\circ\text{S}$ – $70^\circ\text{N}$ ,  $98.5^\circ\text{W}$ – $20^\circ\text{E}$ . In the North Atlantic, its configuration closely resembles that of the WOCE Community Modeling Effort (CME)  $1/3^\circ$  simulation. In the CME model, the eddy field is weaker than in the real ocean, but the model replicates the altimeter-observed poleward decrease in Eulerian length scale ([Stammer and Böning 1992](#)).

The model was spun up for 8 years using the monthly means of the ECMWF climatology (years 79–93), then run for those individual years using daily forcing. Model currents during years 84–88 were integrated using the interpolation technique of [Blanke and Raynaud \(1997\)](#) to produce continuous trajectories for 2480 simulated isobaric Lagrangian floats, at depths from the surface to 4080 m. The simulated floats were “released” at the deployment locations of the actual floats, and Lagrangian eddy scales were calculated from their trajectories as done with the actual floats. Because the simulated drifters and floats never died, they sampled the model ocean more densely than done by the actual drifter/floats.

Eulerian eddy scales were calculated from the model currents during the four years of float simulation. The currents were stored every 4 days at  $1^\circ$  resolution and broken into 120-day segments, each yielding an estimate of  $T_E$  (calculated as with  $T_L$ ). Eulerian length scale  $L_E$  was calculated from monthly current snapshots at the full model resolution. The currents were high passed at 150 days to isolate the eddy field ([Stammer and Böning 1992](#)). Spatial autocorrelation functions of the  $u_i$  were calculated in  $10^\circ$  cells on a grid with  $5^\circ$  overlap (every other cell was independent). These autocorrelation functions were spatially integrated to their first zero crossing and multiplied by two, for consistency with the decorrelation scale  $L_E$  of [Middleton \(1985\)](#).

When presenting Eulerian eddy scales from the model, the “surface layer” is the uppermost model layer and the “deep layer” is the model layer at 1806 m.



## a. Simulated scales in the model

Figure 2 (bottom) shows  $T_L$  and  $L_L$  versus  $u'$  in the model. Simulated  $u'$  are smaller than those observed in the actual ocean by 2–3 times, due to the  $\frac{1}{3}^\circ$  model resolution (Stammer and Böning 1992). Simulated  $L_L$  are also smaller than in the actual ocean.<sup>2</sup> However, the distributions of actual and simulated  $u'$  and  $L_L$  have similar distributions to those in the real ocean (Figs. 3, 5, 6). Simulated and actual  $T_L$  have similar values in the quieter MODE and Eastern basin regions, but simulated  $T_L$  are consistently larger (by 1.6–2 times below the surface) in the Gulf Stream region.

Simulated  $L_E$  decreases with increasing latitude, as in the CME model and in altimetric observations (Stammer and Böning 1992; Stammer 1997). The distribution of simulated  $L_L = u' T_L$  is completely different, primarily mirroring the distribution of  $u'$ . In contrast, simulated  $T_E$  and  $T_L$  are distributed similarly, particularly in the deep layer.

Figure 8 compares the Lagrangian and Eulerian scales in the model. In the deep layer,  $T_L \sim T_E$  and there is no apparent relationship between  $L_L$  and  $L_E$ . The maximum value of  $u' / c_*$  is 0.25, and  $L_L/L_E$  grows linearly with increasing  $u' / c_*$ . In the surface layer,  $u' / c_*$  exceeds unity in some  $10^\circ$  cells. In these high-energy cells,  $T_L/T_E$  drops to 0.5. The linear growth of  $L_L/L_E$  at small  $u' / c_*$  does not persist for  $u' / c_* > 0.5$ .

## 7. Discussion

In the model,  $T_L/T_E$  and  $L_L/L_E$  vary with the nondimensional sampling parameter  $u' / c_*$  approximately as predicted by (9) and (10), although the  $10^\circ$  averages do not fall precisely on the predicted curves (see appendix B). We conclude that the relationship of Middleton (1985) approximately describes the relationships between Lagrangian and Eulerian scales in the primitive equation model, and by extension may apply to the real ocean (at least over the simulated range of  $u' / c_*$ ).

### a. The ocean's sampling regimes

In the model, most of the surface drifters experience fixed-float conditions—the overall median  $u' / c_*$  is 0.23 (Fig. 8). In the most energetic  $10^\circ$  cells, drifters experience intermediate to frozen-field values of  $u' / c_*$ : along the simulated North Atlantic current,  $u' / c_* \sim 0.6$ – $1$ ; in two Gulf Stream cells,  $u' / c_* > 1.2$ . The deep model layer is entirely within the fixed-float regime: maximum values of  $u' / c_*$  are  $\sim 0.2$ ,  $T_L \sim T_E$  in all  $10^\circ$  cells, and  $L_L/L_E$  increases linearly with  $u' / c_*$ .

What sampling regime do actual surface drifters experience? A direct estimate of surface  $u' / c_*$  can be made from drifter-derived  $u'$  and altimetry-derived  $T_E$  and  $L_E$  (Stammer 1997; his Figs. 18b and 21a). This estimate (Fig. 9) suggests that more than half the  $10^\circ$  cells have  $u' / c_* < 1$ , with 10% in the fixed-float range  $u' / c_* < 1/2$ . Frozen-field values ( $u' / c_* > 1$ ) are found along the Gulf Stream, Gulf Stream extension, and North Atlantic Current. Despite potential inconsistencies between definitions of Eulerian scales in Middleton (1985) and Stammer (1997), and contamination by Ekman motion, the ratio of Lagrangian to Eulerian scales are not grossly different from those predicted by Middleton's theory: maximum  $L_L/L_E$  and minimum  $T_L/T_E$  fall in the Gulf Stream extension, where  $u' / c_*$  reaches its maximum of 2.4. Minimum  $L_L/L_E$  and maximum  $T_L/T_E$  coincide with fixed-float ( $< 1/2$ ) values of  $u' / c_*$ .

The deep distribution of Eulerian scales remains unknown, although there are point estimates of  $T_E$  from current meter moorings. In MODE, the Eulerian and Lagrangian timescales were nearly equal (Freeland et al. 1975), consistent with the fixed-float sampling hypothesis. As future concurrent Lagrangian and Eulerian measurements are made, the generality of this behavior should be examined.

### b. Implications for simple empirical rules

If the sampling regime of the mesoscale eddy field varies from frozen field to fixed float, there will be regions described by a nearly constant  $T_L$  or  $L_L$ , as found in previous studies. To demonstrate this, suppose that float observations are collected over a region where the Eulerian scales  $T_E$  and  $L_E$  are nearly constant but the eddy kinetic energy level varies. If  $u' / c_* > 1$  throughout the region, it is in the frozen-field regime where  $L_L = qL_E$  and  $T_L \propto 1/u'$ —there will be a nearly constant Lagrangian length scale  $L_L$ , as found in the near-surface North Atlantic (Krauss and Böning 1987). However, if

$u' / c_* < 1/2$ , the field is in the fixed-float regime where  $T_L \approx T_E$  and  $L_L \propto u'$ —there will be a nearly constant timescale  $T_L$ , as in the MODE and LDE regions (Rossby et al. 1983; McWilliams et al. 1983). If the field is intermediate, both  $T_L$  and  $L_L$  will vary with  $u'$ . This interpretation is consistent with the numerical simulations of Davis (1991), who showed that the Eulerian timescale has a strong influence on eddy diffusivity for small  $u' / c_*$ , and that  $L_E$  and  $u'$  determine  $\kappa_H$  only for large  $u' / c_*$ .

### c. Implications for mesoscale linearity

Davis (1985) noted that the ratio  $T_L/T_E$  varied from unity for deep MODE floats to  $\sim 0.3$  for surface drifters in CODE. He attributed this to the significance of the advection terms in the Eulerian acceleration, with  $T_L/T_E \sim 1$ ,  $L_L \ll L_E$  in a nearly linear field of Rossby waves and  $T_L \ll T_E$  in a fully nonlinear, turbulent field. In this context, Böning (1988) interpreted the sharp decrease in  $L_L$  from 700 m to 1500 m (see Fig. 3) as indicating a transition from a turbulent thermocline to a more wavelike subthermocline. However, although  $T_L \sim T_E$  at 1500 m in MODE, the nonlinearity  $u' / c$  (where  $c$  is the phase propagation speed) was close to unity (Freeland et al. 1975).

To resolve this apparent discrepancy, note that linearity (small  $u' / c$ ) is sufficient to produce fixed-float sampling (small  $u' / c_*$ ,  $c_* = L_E/T_E$ ), but it is not necessary. An eddy field may evolve more rapidly than  $L_E/c$  at a fixed point due to nonlinear interactions— $c_*$  can be significantly larger than  $c$ . This happens in the deep layer of the CLIPPER model, where  $c/c_* < 1/2$  outside the equatorial band (Fig. 10), allowing  $u' / c_* < 1/2$  and  $u' / c \sim O(1)$  over much of the subtropics. Thus, a field of nonlinear, turbulent vortices can produce the fixed-float sampling regime.

## 8. Concluding remarks

It is the Lagrangian, not Eulerian, scales that set absolute dispersion and give the associated eddy diffusivity. If oceanic floats uniformly encountered fixed-float ( $T_L \sim T_E$ ,  $L_L \propto u'$ ) or frozen-field ( $T_L \propto 1/u'$ ,  $L_L \propto L_E$ ) sampling conditions, then one could use  $\kappa_H = u'^2 T_E$  or  $\kappa_H = u' L_E$  (respectively) to calculate meaningful diffusivities directly from Eulerian observations. However, our comparison of Lagrangian and Eulerian scales suggests that the ocean's sampling regime ranges from fixed-float to frozen-field—simple Eulerian-based recipes for  $\kappa_H$  are of dubious value.

In subregions of the ocean where the Eulerian scales are approximately constant and the sampling regime is uniformly fixed-float or frozen-field, a constant  $T_L$  or  $L_L$  can be anticipated. One example is the upper water column in the Gulf Stream: between the surface and 700 m,  $u'$  drops by 1.8 times while  $T_L$  increases by 1.6 times and  $L_L (=u' T_L)$  remains nearly constant, behavior consistent with frozen-field sampling conditions and  $L_E \sim L_L/q \approx 100$  km. In this region of the upper ocean, such conditions would produce a diffusivity of  $\kappa_H = (100 \text{ km})u'$ , which can be mapped directly from Eulerian observations of surface EKE (cf. Stammer 1998).

Perhaps the most striking result of our study is the near-constant  $T_L$  in both the MODE and Eastern basin regions from depth 700 to 2000 m (Fig. 3), a feature that could not be resolved in the absence of recent float observations (cf. Böning 1988). In these regions of the thermocline and subthermocline, one may use

$$\kappa_H \sim (6 \text{ days})u'^2 \quad (11)$$

to estimate a horizontal eddy diffusivity. This may be applicable to the deep ocean more generally, describing the dispersion for several multiples of  $T_L$  (e.g., the 120-day segments). If  $T_L$  is independent of  $u'$  due to fixed-float sampling in these regions, as we have suggested, then  $T_L \sim T_E$  and the deep float observations map the distribution of  $T_E$  at far greater spatial resolution than provided by current meter moorings. Furthermore, a near-constant  $T_E(z)$  suggests that the dynamics of the eddy field may not qualitatively change between the main thermocline and subthermocline, in contrast to the conclusions of Böning (1988). These conclusions need not imply that the deep interior eddy field is nearly linear: the field can be turbulent, that is, characterized by  $O(1)$  nonlinearity, and still produce fixed-float sampling conditions.

### Acknowledgments

Drifter and current meter data were obtained from the WOCE Data Assembly Center. D. Stammer graciously provided Eulerian eddy scales derived from TOPEX/Poseidon observations. We would like to thank B.-L. Hua and B. Le Cann for

many valuable discussions. R. Lumpkin gratefully acknowledges IFREMER for hosting during a French Minister of Foreign Affairs postdoctoral fellowship, and EPSHOM (via the CLIPPER project) for additional funding. Computations were performed at IDRIS (CNRS Computing Center, Orsay, France). Finally, we would like to thank our referees for many valuable comments that helped improve this paper.

---

## REFERENCES

- Batchelor G. K., 1949: Diffusion in a field of homogeneous turbulence: I. Eulerian analysis. *Aust. J. Sci. Res.*, **2A**, 437–450.
- Blanke B., and S. Raynaud, 1997: Kinematics of the Pacific Equatorial Undercurrent: An Eulerian and Lagrangian approach from GCM results. *J. Phys. Oceanogr.*, **37**, 1038–1053. [Find this article online](#)
- Böning C., 1988: Characteristics of particle dispersion in the North Atlantic: An alternative interpretation of SOFAR float results. *Deep-Sea Res.*, **35**, 1379–1385. [Find this article online](#)
- Brink K., R. Beardsley, P. Niiler, M. Abbott, A. Huyer, S. Ramp, T. Stanton, and D. Stuart, 1991: Statistical properties of near-surface flow in the California coastal transition zone. *J. Geophys. Res.*, **96**, 14693–14706. [Find this article online](#)
- Chelton D. B., and M. Schlax, 1996: Global observations of oceanic Rossby waves. *Science*, **272**, 234–238. [Find this article online](#)
- Corrsin S., 1959: Progress report on some turbulent diffusion research. *Advances in Geophysics*, Vol. 6, Academic Press, 161–162.
- Davis R., 1982: On relating Eulerian and Lagrangian velocity statistics: Single particles in homogeneous flows. *J. Fluid Mech.*, **114**, 1–26. [Find this article online](#)
- Davis R., 1985: Drifter observations of coastal surface currents during CODE: The statistical and dynamical views. *J. Geophys. Res.*, **90**, 4756–4772. [Find this article online](#)
- Davis R., 1991: Observing the general circulation with floats. *Deep-Sea Res.*, **38**, 531–571, S. [Find this article online](#)
- Dewar W., 1998: On “too fast” baroclinic planetary waves in the general circulation. *J. Phys. Oceanogr.*, **28**, 1739–1758. [Find this article online](#)
- Fratantoni D. M., 2001: North Atlantic surface circulation during the 1990's observed with satellite-tracked drifters. *J. Geophys. Res.*, **106**, 22067–22093. [Find this article online](#)
- Freeland H., P. Rhines, and T. Rossby, 1975: Statistical observations of the trajectories of neutrally buoyant floats in the North Atlantic. *J. Mar. Res.*, **33**, 383–404. [Find this article online](#)
- Garraffo Z., A. J. Mariano, A. Griffa, C. Veneziani, and E. Chassignet, 2001: Lagrangian data in a high resolution numerical simulation of the North Atlantic. I: Comparison with in situ drifter data. *J. Mar. Syst.*, **29**, 157–176. [Find this article online](#)
- Garrett C., 1994: Dispersion and mixing in the ocean. *Ocean Processes in Climate Dynamics: Global and Mediterranean Examples*, P. Malanotte-Rizzoli and A. R. Robinson, Eds., Kluwer Academic, 61–77.
- Hansen D., and P.-M. Poulain, 1996: Quality control and interpolations of WOCE–TOGA drifter data. *J. Atmos. Oceanic Technol.*, **13**, 900–909. [Find this article online](#)
- Hua B.-L., J. McWilliams, and P. Klein, 1998: Lagrangian accelerations in geostrophic turbulence. *J. Fluid Mech.*, **366**, 87–108. [Find this article online](#)
- Krauss W., and C. Böning, 1987: Lagrangian properties of eddy fields in the northern North Atlantic as deduced from satellite-tracked buoys. *J. Mar. Res.*, **45**, 259–291. [Find this article online](#)
- Lumpkin R., and P. Flament, 2001: Lagrangian statistics in the central North Pacific. *J. Mar. Syst.*, **29**, 141–155. [Find this article online](#)
- McWilliams J., Coauthors, 1983: The local dynamics of eddies in the western North Atlantic. *Eddies in Marine Science*, A. Robinson, Ed., Springer-Verlag, 92–113.
- Middleton J., 1985: Drifter spectra and diffusivities. *J. Mar. Res.*, **43**, 37–55. [Find this article online](#)
- Niiler P., R. Davis, and H. White, 1987: Water-following characteristics of a mixed-layer drifter. *Deep-Sea Res.*, **34**, 1867–1882. [Find this article online](#)
- O'Dwyer J., R. G. Williams, J. LaCasce, and K. Speer, 2000: Does the potential vorticity distribution constrain the spreading of floats in



the North Atlantic? *J. Phys. Oceanogr.*, **30**, 721–732. [Find this article online](#)

Owens W. B., 1991: A statistical description of the mean circulation and eddy variability in the northwestern Atlantic using SOFAR floats. *Progress in Oceanography*, Vol. 28, Pergamon, 257–303.

Poulain P.-M., and P. Niiler, 1989: Statistical analysis of the surface circulation in the California Current System using satellite-tracked drifters. *J. Phys. Oceanogr.*, **19**, 1588–1603. [Find this article online](#)

Qiu B., W. Mao, and P. Müller, 1997: Propagation and decay of forced and free baroclinic Rossby waves in off-equatorial oceans. *J. Phys. Oceanogr.*, **27**, 2405–2417. [Find this article online](#)

Richman J., C. Wunsch, and N. Hogg, 1977: Space and time scales of mesoscale motion in the western North Atlantic. *Rev. Geophys. Space Phys.*, **15**, 385–420. [Find this article online](#)

Rossby H., S. Riser, and A. Mariano, 1983: The western North Atlantic—a Lagrangian view-point. *Eddies in Marine Science*, A. Robinson, Ed., Springer-Verlag, 66–91.

Rupolo V., B.-L. Hua, A. Provenzale, and V. Artale, 1996: Lagrangian velocity spectra at 700 m in the western North Atlantic. *J. Phys. Oceanogr.*, **26**, 1591–1607. [Find this article online](#)

Speer K., J. Gould, and J. LaCasce, 1999: Year-long float trajectories in the Labrador Sea Water of the eastern North Atlantic. *Deep-Sea Res.*, **46**, 165–179. [Find this article online](#)

Stammer D., 1997: Global characteristics of ocean variability estimated from regional TOPEX/Poseidon altimeter measurements. *J. Phys. Oceanogr.*, **27**, 1743–1769. [Find this article online](#)

Stammer D., 1998: On eddy characteristics, eddy transports, and mean flow properties. *J. Phys. Oceanogr.*, **28**, 727–739. [Find this article online](#)

Stammer D., and C. Böning, 1992: Mesoscale variability in the Atlantic Ocean from Geosat altimetry and WOCE high-resolution numerical modeling. *J. Phys. Oceanogr.*, **22**, 732–752. [Find this article online](#)

Swenson M., and P. Niiler, 1996: Statistical analysis of the surface circulation of the California Current. *J. Geophys. Res.*, **101**, 22631–22645. [Find this article online](#)

Taylor G., 1921: Diffusion by continuous movements. *Proc. London Math. Soc.*, **20**, 196–212. [Find this article online](#)

Treguier A.-M., Coauthors, 1999: The CLIPPER project: High resolution modelling of the Atlantic. *International WOCE Newsletter*, No. 36, WOCE International Project Office, Southampton, United Kingdom, 3–5.


Treguier A.-M., Coauthors, 2001: An eddy permitting model of the Atlantic circulation: Evaluating open boundary conditions. *J. Geophys. Res.*, **106**, 22115–22129. [Find this article online](#)

---

## APPENDIX A

### 9. Alternative Methods for Calculating $T_L$

In practice, noise dominates the Lagrangian velocity autocorrelation function  $R$  at large lags. This introduces error when calculating  $T_L$  via (4) and integrating to the maximum record length. The most straightforward solution to this is to truncate the integral at some relatively short lag. Most researchers (cf. [Freeland et al. 1975](#); [Krauss and Böning 1987](#); [Poulain and Niiler 1989](#)) have chosen the decorrelation timescale  $T_D$  (the lag of first zero crossing of  $R$ ), although some have chosen a constant lag (such as 20 d in [Speer et al. 1999](#)). If a constant lag is used, it must fall where noise-induced fluctuations dominate  $R$ , or the resulting  $T_L$  may depend on the physically meaningless value of the constant lag. For this reason, integration to  $T_D$  is more appropriate for large-scale studies where the decorrelation timescales can vary greatly.

In order to avoid truncating the integral in (4), several alternative methods have been proposed to estimate  $T_L$ . In this appendix, three of these methods are applied to the WOCE surface drifter trajectories, broken into 120-day segments and detrended. The resulting distribution of mean  $T_L$  ([Fig. 11](#) ) shows that these alternative methods produce timescales consistent with those of the traditional method used here, indicating that this simplest approach is a robust approximation to (4). We note, however, that this analysis does not explore the additional impact of low-frequency (periods much larger than 120 d) variations removed from the float trajectory segments.

*Squared autocorrelation method.* If the Lagrangian velocity consists of a pure sine wave of period  $P$ , integration to  $T_D$  produces  $T_L = P/2\pi$ . Without this truncation, (4) would fluctuate between  $P/2\pi$  and zero, depending on the record length.

[Richman et al. \(1977\)](#) argued that a pure sine wave should produce an infinite timescale, as it indicates a single process determines  $u(t)$ . This led them to propose an alternative definition for  $T_L$ ,

$$T_L = \int_0^\infty d\tau R^2(\tau). \quad (\text{A1})$$

As noted by Richman et al., this definition tends to produce longer timescales than (4), even with truncation at  $T_D$ . This method has a distinct disadvantage: noise-induced fluctuations tend to cancel when integrated over  $R$ , but always increase  $T_L$  in an integral over  $R^2$ . Thus, (A1) will produce  $T_L$  that are a function of record length if the noise-induced component of (A1) is significant compared to the signal-induced component.

For the drifters, this method produces  $T_L$ , which are on average 1.2 times greater than those presented here. Taking this factor into account, the two calculations yield similar maps of  $T_L$ .

*Fitting a prescribed autocorrelation function.* In their calculation of  $T_L$  from drifter data, [Garraffo et al. \(2001\)](#) fit an autocorrelation function of the form

$$R^*(\tau) = \cos\left(\frac{\pi\tau}{2T_D}\right) e^{-(\tau/\tau_e)^2} \quad (\text{A2})$$

to the observed  $R$ , using the first zero crossing of  $R$  to set  $T_D$  and determining the  $e$ -folding timescale  $\tau_e$  via a least squares fit. They used the exact integral of this function to infinite lag to get  $T_L$ :

$$T_L = \int_0^\infty d\tau R^*(\tau) = \frac{\sqrt{\pi}}{2} \tau_e e^{-(\pi\tau_e/4T_D)^2}. \quad (\text{A3})$$

The traditional method of calculating  $T_L$  gives  $T_L \sim T_D/2$ . For fixed  $T_D$ , (A3) reaches a maximum for  $\tau_e/T_D = 2(2)^{1/2}/\pi \approx 0.9$ , for which  $T_L = (2/\pi)^{1/2} e^{-1/2} T_D \approx 0.48T_D$ . Smaller  $\tau_e$  cause  $R^*$  to have an extremely narrow positive lobe, while larger  $\tau_e$  produce deeper negative lobes; both effects reduce  $T_L$ .

For the average WOCE drifter,  $\tau_e \sim 0.89T_D$  and the overall mean of  $T_L$  is 1.02 times larger than  $T_L$  from the traditional calculation. In the subtropics,  $\tau_e/T_D \sim 1.2$ – $1.3$ , reflecting the presence of a stronger negative lobe in  $R$ , perhaps due to more wavelike dynamics at these latitudes. The effect on  $T_L$  is subtle: south of  $30^\circ\text{N}$ , it is smaller than in the traditional calculation by only 1.03 times. Thus, the map of surface  $T_L$  in [Garraffo et al. \(2001\)](#) strongly resembles the map of [Fig. 4](#)

☞.

*Yardstick method.* [Rupolo et al. \(1996\)](#) proposed a unique method for calculating  $T_L$  that completely avoids integrating an autocorrelation function. In their method, a drifter trajectory's length is measured by a “yardstick” of fixed length  $\Delta$  in a frame of reference moving at the mean drifter speed. The resulting measurement,  $\mathcal{L}(\Delta)$ , is always smaller than  $\mathcal{L}(\Delta = 0)$  because of smoothing at scales smaller than  $\Delta$ . When  $\Delta$  is much larger than the eddy length scale, decreasing  $\Delta$  causes a relatively fast increase in  $\mathcal{L}(\Delta)$ . However, as  $\Delta$  approaches the eddy length scale, the yardstick is applied over a distance for which  $u$  remains correlated with itself, so the measured trajectory length  $\mathcal{L}(\Delta)$  asymptotically approaches the constant value  $\mathcal{L}(0)$ . The transition between the fractal behavior of  $\mathcal{L}(\Delta)$  at  $\Delta \gg L_L$  and  $\mathcal{L}(\Delta) \sim \mathcal{L}(0)$  at  $\Delta \leq L_L$  thus gives an estimate of the eddy length scale. The yardstick length scale  $L_{\text{yard}}$  can be defined as

$$\mathcal{L}(L_{\text{yard}}) = \frac{2}{\pi} \mathcal{L}(0), \quad (\text{A4})$$

so a perfectly circular drifter trajectory of diameter  $D$  will have  $L_{\text{yard}} = D$ . The integral timescale can then be defined as

$$T_L = \mu L_{\text{yard}} / u' \quad , \quad (\text{A5})$$

where the constant  $\mu$  is chosen to produce mean scales consistent with (4) (Rupolo et al. 1996). For the surface drifters, we find  $\mu = 0.40$ . The yardstick method produces  $T_L$  that span a wider range of values than via the traditional method: subtropical maxima are  $\sim 1.05$  times larger, while subpolar minima are  $\sim 1.1$  times smaller. Qualitatively, the distribution of yardstick-derived  $T_L$  is similar to that of the traditional method.

## APPENDIX B

### 10. Sources of Error

The ratio of Lagrangian to Eulerian scales in the model tend to obey (9) and (10), but with considerable scatter for the  $10^\circ$  averages. Sources of this scatter include:

*Violation of the theory's assumptions.* Middleton's theory assumes the motion is nondivergent, which is not the case for floats constrained to a constant-pressure layer in the simulated or actual ocean. The theory also assumes that the Eulerian statistics are stationary and homogeneous. In the model, as in the actual ocean, eddy energy and scales change in space and time. We have attempted to minimize these effects via  $10^\circ$  cell averages, but cannot eliminate them entirely. For example, float trajectories have been broken into 120-day segments in this study. Had a shorter duration been chosen, the trajectories would be shorter and thus less sensitive to large-scale inhomogeneities. However, the energy-containing eddy band is  $\sim 50$ – $150$  day in Eulerian spectra (Richman et al. 1977), and thus should be at similar periods in fixed-float Lagrangian spectra. Because the eddy band is red, shorter time series can produce shorter timescales that are a function of the record length. Thus, comparing Eulerian and Lagrangian scales in the ocean will inevitably require a balance between neglecting the red end of the eddy spectrum (producing artificially shortened timescales, especially in the fixed-float regime) and introducing errors due to inhomogeneity.

*Measurement error.* Eddy scales calculated from a finite time series are only approximations to the true integral scales, for which Middleton (1985) applies (see appendix A). The overall distribution of the eddy scales is not strongly sensitive to this approximation, but values in individual  $10^\circ$  cells can vary considerably. Thus, the finite-time approximation to (4) introduces some scatter to the eddy scales.

*Theoretical inaccuracy.* As noted by Middleton, Corrsin's conjecture (Corrsin 1959) is accurate only when the Eulerian and Lagrangian timescales are of the same order. Thus, the theory (which relies on this conjecture) may be systematically incorrect in the limit  $u' / c_* \gg 1$ . Such behavior is not apparent in the  $1/3^\circ$  model (Fig. 8  $\bullet$ ), but this may be due to the limited range of  $u' / c_*$ . Higher resolution models will be able to resolve this issue in future studies.

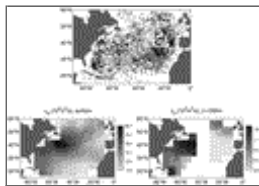
*Doppler-shifting of the Eulerian timescale.* Relation (9) assumes that the eddy field is not moving. However, oceanic mesoscale features drift westward (Chelton and Schlax 1996) due to  $\beta$ -induced free propagation, with variations from linear theory caused by advection by mean currents, alteration of the local planetary vorticity by mean shear, the superposition of forced waves, and a host of other possible mechanisms (cf. Qiu et al. 1997; Dewar 1998). This drift can shorten the apparent timescale for fixed observers. For example, consider the extreme case of an unchanging (frozen) field drifting at speed  $c$ : the Eulerian timescale is  $T_E = L_E/c$ , but in the reference frame moving at  $c$  the apparent Eulerian timescale (for which Middleton's relationships are formulated) is  $T'_E = \infty$ . If the mesoscale field is evolving,  $T'_E$  is finite and  $T_E$  satisfies  $T_E < L_E/c$ . Middleton (1985) suggested a relationship of the form

$$T'_E \sim T_E \left[ 1 - \left( \frac{c}{c_*} \right)^2 \right]^{-1/2} \quad , \quad (\text{B1})$$

which satisfies  $T'_E \rightarrow \infty$  for  $T_E \rightarrow L_E/c$  and  $T'_E \rightarrow T_E$  for  $c/c_* \rightarrow 0$ . In the surface model layer, mesoscale disturbances drift westward at speeds close to the first baroclinic Rossby wave speed (Fig. 10  $\bullet$ ) (the model does not appear to replicate the discrepancy with linear theory noted by Chelton and Schlax 1996). Except near the model's equator,  $c$  is generally much smaller than the evolution speed  $c_*$ ; thus, eddy fluctuations look similar in the fixed, Eulerian frame and in a frame moving at  $c$ . Few  $10^\circ$  cells have  $|c/c_*|^2 > 0.2$ , suggesting that Doppler-shifting is not a major source of scatter.

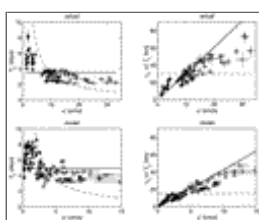
Scatter inherent in the theory. Middleton derived (9) for a particular Eulerian field, but found that the ratio  $T_L/T_E$  as a function of  $u' / c_*$  varied by  $\sim 10\%$  for widely ranging Eulerian statistics. Because the model Eulerian field has spatially varying length and timescales, similar scatter could appear in Fig. 8 without appealing to any of the previous arguments.

## Figures



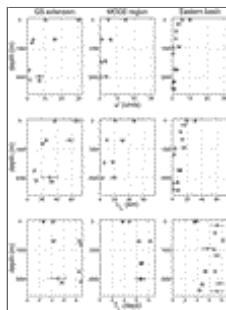
Click on thumbnail for full-sized image.

FIG. 1. (Top) median positions for 120-day segments of drifter and float trajectories at the surface (open circles), subsurface to depth 1500 m (gray stars), and deeper than 1500 m (black stars). Boxes indicate regions isolated in Fig. 3. Bottom: apparent eddy diffusivity from surface drifters (left) and floats below 1500 m (right)



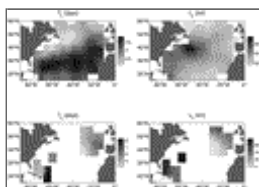
Click on thumbnail for full-sized image.

FIG. 2. Lagrangian time (left) and length (right) eddy scales vs eddy speed, for actual (top) and simulated (bottom) float trajectories. Open circles are at the surface, filled points are in the deep layer (1700–2000 m). The scales have been averaged in  $10^\circ$  cells; standard error bars (thin lines) are calculated from the scatter of values within each cell. Heavy solid lines show the distributions if  $T_L$  were constant everywhere (the overall mean is used). Dashed lines show the distributions if  $u' T_L = L_L$  were constant everywhere (the overall mean of  $L_L$  is used)



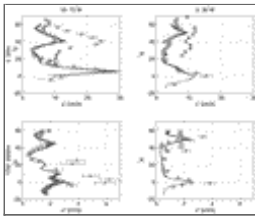
Click on thumbnail for full-sized image.

FIG. 3. Lagrangian eddy speed (top) and length (middle) and time (bottom) scales as a function of depth for the actual (asterisks) and simulated (circles) floats. Each column corresponds to a region shown in Fig. 1. Standard error bars are indicated



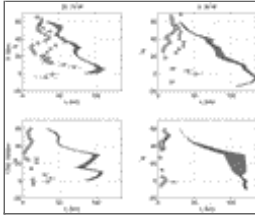
Click on thumbnail for full-sized image.

FIG. 4. Lagrangian eddy scales observed by surface (top) and deep (bottom) drifters and floats. The time (left) and length (right) scales have been averaged in  $10^\circ$  cells



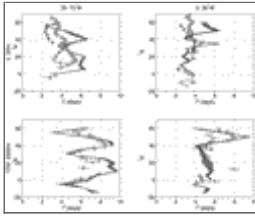
Click on thumbnail for full-sized image.

FIG. 5. Lagrangian eddy speed  $u'$  as a function of latitude for the actual (asterisks) and simulated (circles) floats, with standard error bars. The zonal averages are conducted separately for surface (top) and deep (bottom) observations and data west of  $35^\circ\text{W}$  (left) and east of  $30^\circ\text{W}$  (right). Solid lines with shaded error bars indicate zonally averaged  $u'$  from the high-passed model output, weighted by the mean density of simulated Lagrangian observations



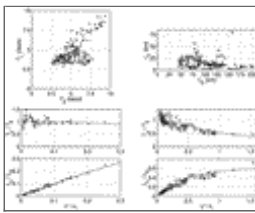
Click on thumbnail for full-sized image.

FIG. 6. Lagrangian length scale  $L_L$  as a function of latitude for the actual (asterisks) and simulated (circles) floats, with standard error bars. The zonal averages are conducted separately for surface (top) and deep (bottom) observations and data west of  $35^\circ\text{W}$  (left) and east of  $30^\circ\text{W}$  (right). Solid lines with shaded error bars indicate zonally averaged  $L_E$  calculated from the high-passed model output, multiplied by  $q = (\pi/8)^{1/2} \sim 0.63$  and weighted by the mean density of simulated Lagrangian observations



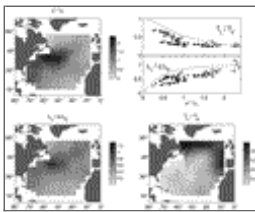
Click on thumbnail for full-sized image.

FIG. 7. Lagrangian timescale  $T_L$  as a function of latitude for the actual (stars) and simulated (circles) floats, with standard error bars. The zonal averages are conducted separately for surface (top) and deep (bottom) observations and data west of  $35^\circ\text{W}$  (left) and east of  $30^\circ\text{W}$  (right). Solid lines with shaded error bars indicate zonally averaged  $T_E$  calculated from the high-passed model output, weighted by the mean density of simulated Lagrangian observations



Click on thumbnail for full-sized image.

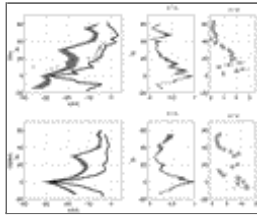
FIG. 8. A comparison of Lagrangian and Eulerian scales in the surface (open circles) and deep (filled points) layers of the model. Each point is a  $10^\circ$  average. Top Lagrangian time (left) and length (right) scales vs their Eulerian counterparts. Bottom ratio of Lagrangian to Eulerian length (left) and time (right) scales vs the sampling regime parameter  $u'/c$ . Solid lines show the theoretical ratio (Middleton 1985)



Click on thumbnail for full-sized image.

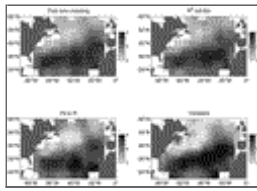


FIG. 9. A comparison of Lagrangian and Eulerian scales at the ocean surface. Eulerian scales are from [Stammer \(1997\)](#) (his Figs. 18b and 21a), averaged in  $10^\circ$  cells. Top, left: Distribution of  $u' / c_*$  ( $u'$  from surface drifters). Top, right:  $T_L/T_E$  (upper) and  $L_L/qL_E$  (lower),  $q = (\pi/8)^{1/2}$ , as a function of  $u' / c_*$ . Bottom, left: Distribution of  $L_L/qL_E$ . Bottom, right: Distribution of  $T_L/T_E$



[Click on thumbnail for full-sized image.](#)

FIG. 10. Left: zonally averaged ( $0^\circ$ – $60^\circ$ W) evolution speed  $c_* = L_E/T_E$  (shaded error bar) in the model surface (top) and deep (bottom) layers. The westward drift speeds  $c$  of mesoscale fluctuations are also shown (heavy lines), calculated from Hovmöller diagrams (eddy energy as a function of longitude,  $0$ – $60^\circ$ W, and time) averaging  $2^\circ$  of latitude. For reference, circles give propagation speeds derived from altimetry ([Chelton and Schlax 1996](#)). Middle: Ratio of propagation speed  $c$  to evolution speed  $c_*$  in the model. Right: ratio of propagation speed  $c$  to rms eddy speed  $u'$  in the model



[Click on thumbnail for full-sized image.](#)

FIG. 11. The distribution of eddy timescale  $T_L$  (days) for the WOCE surface drifters, calculated by four different methods (see [appendix A](#)). Top, left: the observed autocorrelation function is integrated to the first zero crossing. Top, right: The squared autocorrelation function method ( $T_L$  multiplied by 0.84). Bottom, left: The prescribed autocorrelation function method. Bottom right: The yardstick method

<sup>1</sup> For a tabulation of these data, see [O'Dwyer et al. \(2000\)](#).

<sup>2</sup> Simulated length scales much smaller than  $1/3^\circ$  in a  $1/3^\circ$  model may seem paradoxical, but are not: float displacements by the interpolated velocity field can be subgrid scale in the fixed-float regime. Eulerian scales, on the other hand, cannot be (and are not) subgrid scale.

Corresponding author address: Rick Lumpkin, Dept. of Oceanography, The Florida State University, Tallahassee, FL 32306-4320. E-mail: [rlumpkin@ocean.fsu.edu](mailto:rlumpkin@ocean.fsu.edu)

[top ▲](#)



© 2008 American Meteorological Society [Privacy Policy and Disclaimer](#)  
 Headquarters: 45 Beacon Street Boston, MA 02108-3693  
 DC Office: 1120 G Street, NW, Suite 800 Washington DC, 20005-3826  
[amsinfo@ametsoc.org](mailto:amsinfo@ametsoc.org) Phone: 617-227-2425 Fax: 617-742-8718  
 Allen Press, Inc. assists in the online publication of AMS journals.